Proceedings of ASME Turbo Expo 2011
GT2011
June 6-10, 2011, Vancouver, British Columbia, Canada

GT2011-46616

OVERALL AND ADIABATIC EFFECTIVENESS VALUES ON A SCALED UP SIMULATED GAS TURBINE VANE:-PART II-NUMERICAL SIMULATIONS

GUSTAVO A. LEDEZMA
GE Global Research Center
Niskayuna, NY USA

GREGORY M. LASKOWSKI
GE Global Research Center
Niskayuna, NY USA

JASON E. DEES
The University of Texas at Austin
Austin, Texas USA

DAVID G. BOGARD
The University of Texas at Austin
Austin, Texas USA

ABSTRACT

Conjugate heat transfer (CHT) calculation techniques for the heat transfer analysis of high-pressure turbines (HPT) have been developed during the past few years. Thus, it has become possible to take into account the coupling of the film, internal cooling, external gas flow and the metal diffusive heat transfer. The coupling problem may become extremely important in regions such as the airfoil leading edge and the vicinity of film hole breakout region where heat fluxes and thermal gradients are high. This article presents the results obtained using fully coupled 3D CHT simulations of a simplified film-cooled leading edge model and a NASA C3X vane with suction side film cooling. The results for the two cases are compared against experimental data obtained at University of Texas at Austin. The numerical simulations were conducted using the k-ω turbulence model. The leading edge model overall effectiveness predictions are in good agreement with the experiments, especially in the low blowing ratio range ($1 \leq M \leq 2$). For the C3X vane, the CHT results tend to underpredict the midspan and laterally averaged effectiveness due to film liftoff. However, the quantitative agreement is still reasonably good. The different levels of overall effectiveness agreement found between all cases are discussed.

INTRODUCTION

New advances in Computational Fluid Dynamics (CFD) have made it increasingly more accepted as a commonly used tool by the gas turbine research and design community. The advances include not only better and more robust turbulence models and highly efficient linear solvers but also a rapid increase in computer power. Such advances have made CHT a potentially attractive design and analysis tool, not immediately but possibly within the next few years. CHT eliminates the need for iterating between various design tools to obtain the heat transfer information that would ultimately be used for lifing analysis. Its coupled nature leads to better capturing of the physics in complicated internal passages and tip-cooling flows that otherwise would have been approximated with 1-D or reduced order analyses. Film cooling, for example, is often modeled using source terms or other semi-empirical techniques that usually have limited success and lack of universality. In most cases, semi-empirical film cooling models need to be calibrated to the variety of film cooling holes shapes, locations and flow conditions in which they have to operate.

Turning CHT into a reliable and efficient analysis and design tool is a challenging endeavor. Some of the main challenges include the difficulty of finding grid independent solutions with unstructured meshes, limitations of RANS turbulence models to accurately predict film cooling and the lack of good quality validation data for realistic turbine configurations. Previous CHT validation efforts have used simplified internal cooling geometries such as radial cooling channels with air [1-3], and steam cooling [4,5]. Bucchieri et al. [5] carried out CHT computations in a shrouded turbine

blade that focused on the optimization of tip cooling holes layouts. In refs. [6,7] CHT was applied to blade cooling configurations that included complex serpentine passages and film cooling. These studies used a simple algebraic turbulence model and some geometric simplifications. Despite the simplifications made and the uncertainty in the hot gas boundary conditions, the numerical results compared favorably against thermal paint data. Montomoli et al. [8] solved the CHT problem in a film cooled transonic vane. The CHT Nusselt number predictions agreed well with experimental data, especially on the pressure side of the vane. Takahashi [9] carried out CHT calculations in a rotor blade with rib-roughened internal cooling passages using a commercial code. The conjugate model consisted of hot gas and metal blade while the internal passages were modeled using 1-D correlations. The numerical results were compared against distinctive features of damage in ex-service blades and ex-service blade temperature estimates based on micro-structural changes. In a recent paper Laskowski et al. [2] was successful in accurately predicting the metal temperatures of the film cooled NASA C3X [10] using a fully coupled CHT model. However, a direct validation in the vicinity of the film cooling holes could not be made because the measurements of Hylton et al., [10] were only available downstream of the 30% axial coordinate location in both the pressure and suction sides. Since the highest thermal gradients and heat fluxes are found in the vicinity of the film cooling holes and the leading edge regions, it becomes critical to assess the predictive capabilities of any CHT technique in those regions. More recently Dees et al. [19-21] carried out measurement of overall effectiveness in a scaled C3X vane with internal cooling. This work included details of both external (IR) and internal temperature distributions. Numerical simulations were carried out simultaneously with varied levels of agreement depending upon suction side boundary layer transition and other factors.

In this article, efforts have been undertaken to investigate the predictive capability of a fully coupled CHT technique in film-cooled airfoil models. Two cases were studied: the leading edge film cooled vane model of Albert and Bogard [12] and the suction side film cooling IR measurements made in a NASA C3X vane model at UTA [19-21] and presented in the first part of this paper. The numerical domains include external flow, internal and film cooling and metal. The objective was to assess the predictive capability of a CHT approach for film cooling configurations on highly curved surfaces that are typically encountered in high-pressure turbine vanes and nozzles.

NOMENCLATURE

Bi =Biot Number, $\frac{h_e t}{k}$

h = heat transfer coefficient

I = momentum ratio, $\frac{\rho_c U_c^2}{\rho_g U_g^2}$

k = thermal conductivity

t = thickness of vane wall = 1.27 cm

Re = Reynolds number

s = streamwise surface distance from stagnation

T = temperature

Tu = Freestream turbulence intensity

U = flow velocity

x =streamwise coordinate

z =spanwise distance from bottom of vane

Greek

ϕ = Overall effectiveness, $\phi = \frac{T_\infty - T_w}{T_\infty - T_c}$

ν = kinematic viscosity

η = adiabatic effectiveness, $\eta = \frac{T_\infty - T_{aw}}{T_\infty - T_f}$

Subscripts

c = coolant

C = true chord of airfoil

f = at hole exit

g = local gas

int = internal coolant

∞ = freestream

FILM COOLING MODELS

Case 1 – Leading Edge Model

The conjugate leading edge model of Albert et al., [12] was investigated at three blowing ratios, M=1, 2 and 4. The solid vane thermal material used in the numerical model was alumina with a thermal conductivity of 1.4 W/mK. The hot gas consisted of air at ambient conditions.

Two domains were constructed and meshed independently for the solid airfoil, and the fluid region (hot gas path, plenum and film holes). The computational domain is shown in Fig. 1. The hot gas flows in the negative X direction. The leading edge model has 3 rows of 9 forward diffused, compound angle cooling holes each (Fig. 2). The cooling holes are oriented in the positive Z direction (Fig. 1b). The velocity, U_∞ = 20 m/s and static temperature, T_∞ = 25°C were prescribed at the hot gas path inlet whereas static pressure was prescribed at the hot gas domain exit. Adiabatic walls were assumed for the wind tunnel walls. Mass flow rate and static temperature, T_{in} = -110 deg C, were set at the inlet of the plenum feeding the film holes. The mass flow was adjusted to arrive at the desired blowing ratio as shown in Table 1. Conjugate heat transfer boundary conditions were utilized along both the plenum-side and blade-side wall surfaces.

Table 1. Plenum inlet mass flow

Blowing ratio, M	Mass flow [kg/s]
1	0.00505
2	0.01010
4	0.02020

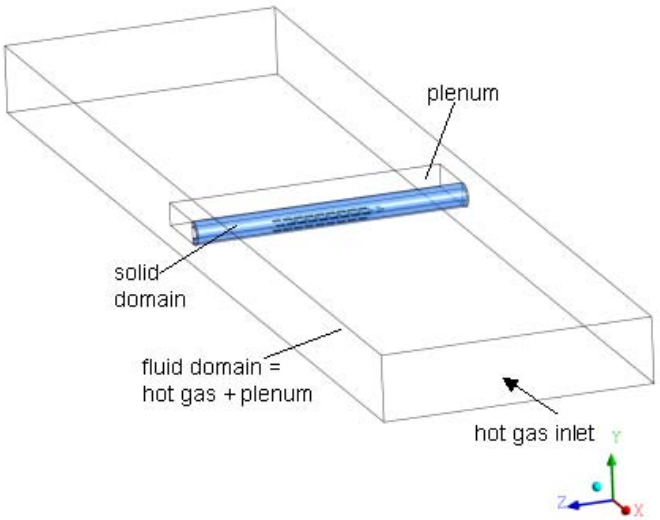

(a)

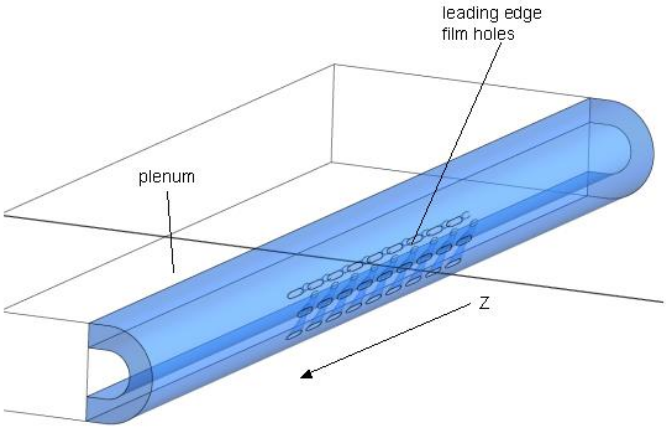

(b)

Figure 1. Leading edge model. Computational domain. (a) Complete domain; (b) Detail of the solid domain

The overall dimensions of the leading edge/plenum computational domain match exactly the experimental facility [11]: 0.61 m wide (spanwise) 0.051 m tall and 0.18 m long (mainstream flow direction). The plenum inlet boundary condition is located on the face opposite to the leading edge.

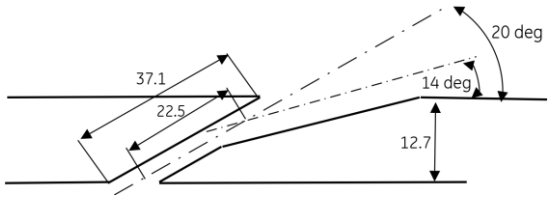

(a)

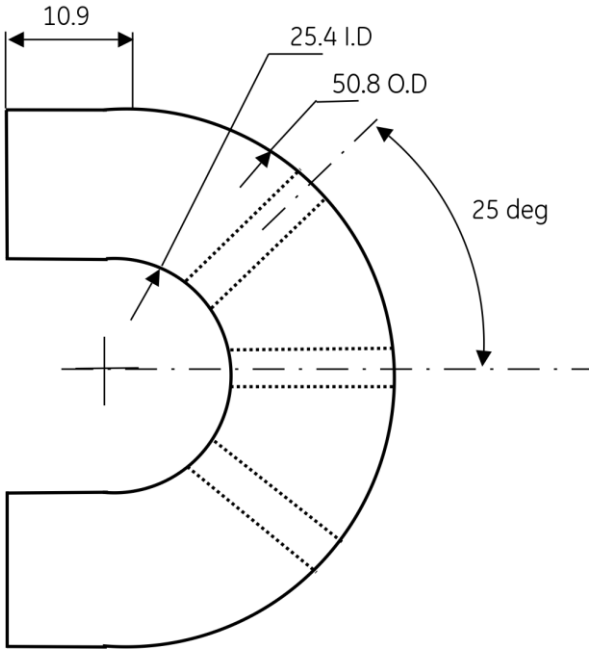

(b)

Figure 2. (a) Cross section of a single cooling hole. Through hole and expansion hole are both 3.18 mm in diameter; (b) Side view of the solid (leading edge) model. Units are in mm. Ref [11]

Case 2 – HPT vane with suction side film cooling

The vane model consists of a NASA C3X airfoil [10] scaled up 3.88 times. The called up vane has a true chord C=56.2 cm and a spanwise height of H=54.7 cm. The pitch between the vanes is 45.7 cm. The test airfoil used was constructed out of a high conductivity, castable epoxy resin that had thermal conductivity of k = 1.02 W/m*K. This material was selected in order to match the Biot number of the model to the Biot number of an engine component. Matching the Biot number is required in order to match the non-dimensional temperature distribution that would be present on an actual engine component [19-21]. The internal cooling circuit consists of two internal cooling cavities, a U-bend cavity in the forward part of the vane and a radial cooling channel in the aft region (see Fig. 3b). A single row of 24 suction side cylindrical film hole are located at s/d=0.21. The holes had an angle of 42-degrees with respect to the vane tangent. The internal cooling flow Reynolds numbers based on the hydraulic diameter was kept at 20,000 for all simulations. The prescribed inlet temperature was 250 K and a turbulence intensity of 5% was used. The inlet flow conditions for the external flow were U=5.8 m/s, T=300 K and TU=0.5%. The corresponding chord base Reynolds number is 750,000. Details of the computational domain are given in Fig. [3]. More details of the experimental facility are given in refs. [20-21] and in part I of this paper.

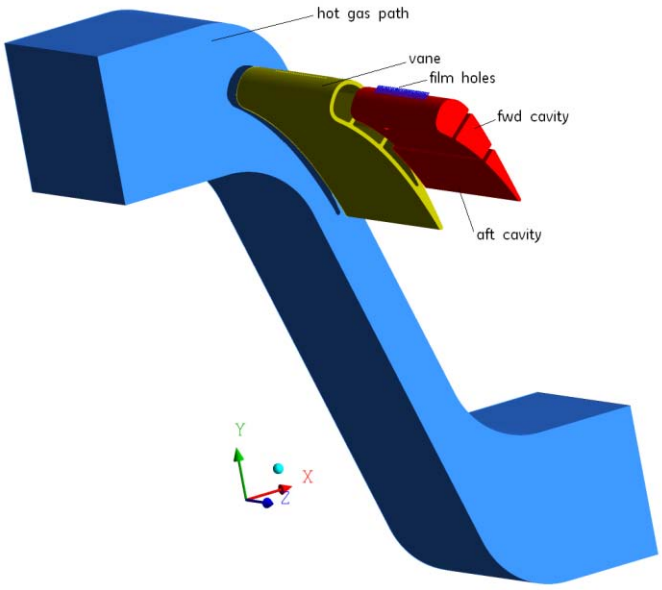

(a)

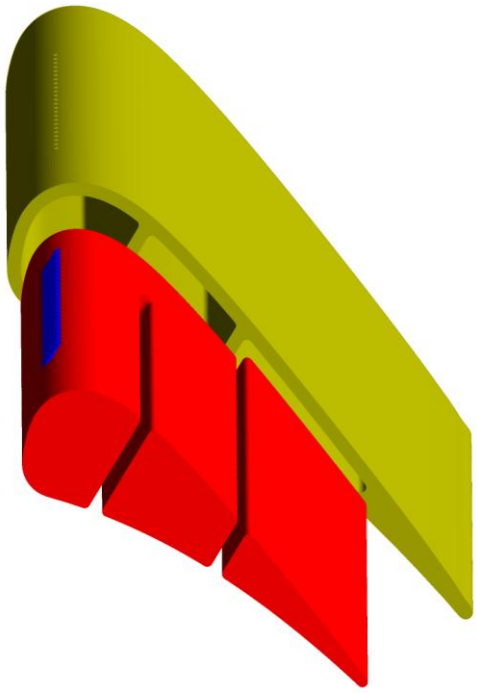

(b)

Figure 3. Computational Domains: (a) 5 Domains; (b) Detail of vane and cavities

NUMERICAL METHODOLOGY

Steady-state solutions of the conservation equations for mass momentum and energy and turbulence closure transport equations were solved using CFX v11.0 [13]. The air was modeled as a perfect gas with constant specific heat while the temperature-dependent thermal conductivity and viscosity were modeled using Sutherland's formula. Unstructured wall integration grids were used which consisted of inflated layers of prismatic elements grown near the solid wall surfaces to accurately resolve the boundary layers. The prismatic elements transitioned into tetrahedral elements via pyramidal and wedge elements. All grids are wall integration ($y+ < 1$).

For the Leading edge model a single fluid domain was used. The grid included the hot gas path, plenum and film holes. The solid constituted a separate domain that was meshed independently. The mesh interface between the solid and fluid consisted of non-conforming nodes that required the use of solid-fluid general grid interface (GGI) feature from CFX. This approach has previously been validated in similar CHT analyses [2,17]. For case 2, the film holes were split at the hot gas and cavity interfaces so the holes could be meshed separately. A fluid/fluid non-conforming generalized grid interface (GGI) was prescribed at the interface between the plenum and film domains and the film and hot gas domains. The mesh statistics are summarized in Table 2. Figure 3 shows each of the computational domains that were meshed separately.

Grid independence studies were carried out for both the leading edge and the C3X vane model. In the leading edge model 2 meshes with 7 and 21 million elements respectively were tested. The refinement was made in the vicinity of the leading edge region of the fluid mesh. No significant differences were found between the 2 solutions. All results are reported on the 7 million elements mesh. The grid refinement on the C3X vane focused on the hot gas path near the film hole breakout region. A detail of the 2 hot gas path meshes is shown in Fig. 4. Figure 5 depicts the effect of the aggressively increased grid density near the hole interface on the adiabatic effectiveness. Although results become closer to the experimental data downstream of $S/d \cong 15$, the CFD-predicted adiabatic effectiveness fails to predict the experimental data slope. Previous attempts to numerically predict laterally averaged adiabatic effectiveness have shown similar results. For example, in the leading edge model of ref. [24] the numerical effectiveness decays rapidly while experimental one remains nearly constant for x/D between 6 and 12. Other example can be found in ref. [26] where the authors attempted to validate their numerical method using experimental data from a periodic single cylindrical hole on a flat plate. In this case the laterally averaged effectiveness is not only underpredicted by approximately 25% but also the numerical and experimental slope of the effectiveness curves are different along the streamwise coordinate from x/D=2 to 15. Unless specified all reported results correspond to mesh 1.

Table 2. NASA C3X model meshes

Domain	Number of elements
Hot Gas Path (1)	15,119,621
Vane	10,464290
Fwd Cavity	4,150,158
Aft Cavity	7,293,692
Holes	2,455,247
Hot Gas Path (2)	21,730,696

The Wilcox k-ω turbulence model with a Kato-Launder production limiter was used in all the simulations [13]. The advection term in all the conservation equations was treated using CFX high-resolution scheme except for the turbulence transport equations where a first-order upwinding scheme was used.

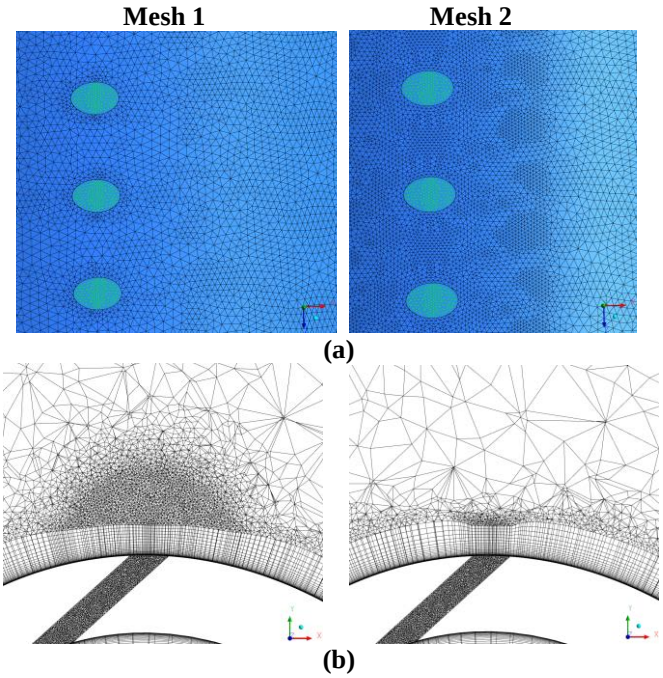

Figure 4. Mesh density near the film holes. HGP mesh 1 (left), mesh 2 (right)

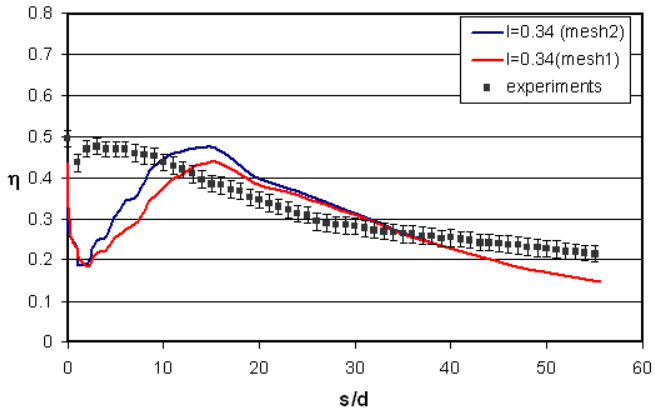

Figure 5. Effect of local mesh refinement near the film row. Adiabatic effectiveness, I=0.34

RESULTS

Leading Edge Model

The overall effectiveness (ϕ) contours at the leading edge for all blowing ratios are summarized in Fig. 6. The definition of overall effectiveness includes the effect of film cooling, internal cooling and conduction in the solid. The radial coolant jet orientation is in the positive Z direction. For all blowing ratios the film hole row located at the stagnation line is not swept downstream as fast as the off-stagnation rows. As the blowing ratio increases the overall effectiveness footprint downstream of the off-stagnation rows become more pronounced. The contours also indicate that the overall cooling effectiveness increases with the blowing ratio. This trend is better observed in Fig. 7 where the numerical and experimental laterally averaged overall effectiveness are plotted as a function of the streamwise coordinate of the airfoil surface, s/d. The agreement between CFD and experiments is within the experimental uncertainty downstream of the off-stagnation film row, for blowing ratios equal to 2 and 4. However, when M=1 the overall effectiveness is underpredicted by up to 22% at s/d=10. In the region between film rows (0.5<s/d<3) significant differences show up between numerical end experimental results. The experiments predict a nearly constant laterally averaged overall effectiveness while the CFD predicts a ~15% decrease from the exit of the leading edge row to the off-stagnation row. A similar behavior was observed in another leading edge numerical investigation [24]. The numerical results reported in ref. [24] predict a 20% lower laterally averaged adiabatic effectiveness at the leading edge hole exit. The authors attributed these discrepancies to RANS limitations. The nearly constant overall effectiveness near the leading edge region observed in the experimental results (Figs. 7-9) is attributed to the internal cooling contribution to the effectiveness [12]. The diffusion in the solid is smearing out the local temperature gradients that otherwise would be produced by the film cooling. The effectiveness differences between CFD and experimental data in the leading edge region could be the product of not properly resolving the internal convection in the cooling holes due to local mesh quality, differences in the experimental and numerical geometries including sharp edges and roughness, and RANS turbulence model limitations observed in previous studies [15,22,24]. It is worth noting that the good agreement found downstream of s/d=4 indicates that both plenum convection and external film heat transfer are properly captured by the CFD in this region.

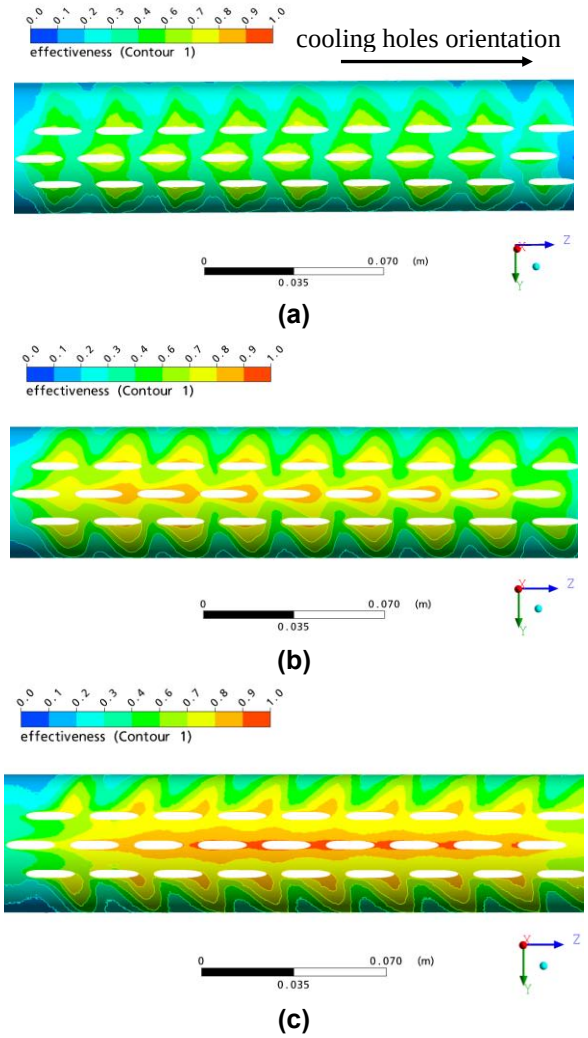

Figure 6. Overall effectiveness contours for different blowing rations. (a) M = 1; (b) M = 2; (c) M = 4

The most recent attempts to model leading edge film cooling and compare against experimental data are refs. [24-25], and [27-28]. The studies in refs. [24-25] did not include conjugate effects, and the blowing ratio varied between 1 and 2. As in the present study, the predicted laterally averaged effectiveness between rows failed to capture the experimental data slope. The studies by Ravelli [27] and Dobrowolski [28] did include conjugate effects and used a similar film cooling hole configuration as the present study. The predictions in ref. [28] used a measured internal temperature boundary condition so that the prediction of the internal cooling was not required. The blowing ratios were 1 and 2. For this case, the predicted laterally-averaged effectiveness between rows of holes is approximately 20% higher than the data and shows a negative slope similar to the results of the present study (Fig. 7). However, downstream of the off-stagnation row, Dobrowolski's results did not match the slope of the laterally averaged effectiveness curve. The numerical simulations of leading edge film cooling in ref. [27] are similar to those of ref. [28] but explicitly model the internal wall impingement cooling. The quality of laterally averaged effectiveness predictions between holes varies with the blowing ratio. Good agreement is found for M=2 . However when M=1, the effectiveness is underpredicted by more than 25%. Downstream of the off-stagnation row the agreement is good for the two studied blowing ratios.

A comparison between the CHT effectiveness contours in the leading edge and the results from ref. [12] is shown in Fig. 8 for M ≈ 2.0. Although the effectiveness color maps are different, a good qualitative agreement can be observed. The more uniform experimental overall effectiveness between stagnation and off-stagnation rows is also evident and clarifies the almost constant slope in the experimental curves of Fig. 7 versus the decaying effectiveness shown in the numerical results. Figure 9 shows the effectiveness-colored streamlines emerging from the holes and the effectiveness contours on the leading edge. The streamlines show the interaction between the stagnation and off stagnation film rows. The relationship between the film cooling flow and the effectiveness footprint is also apparent.

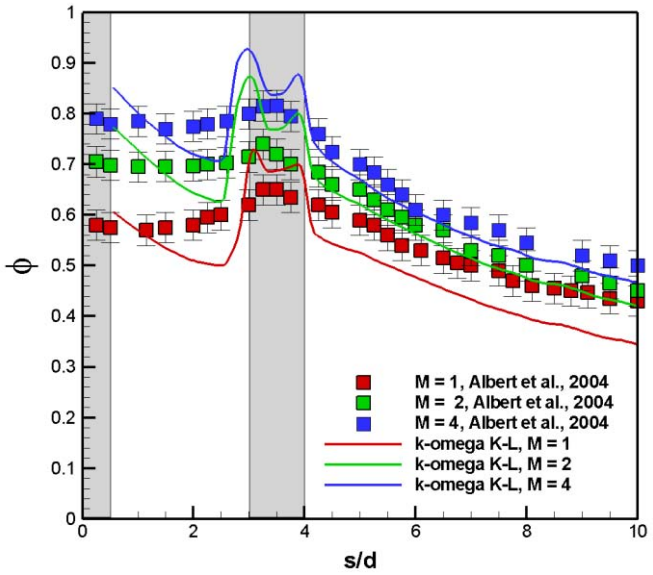

Figure 7. Laterally averaged overall effectiveness for different blowing ratios. The gray bands indicate the position occupied by film holes

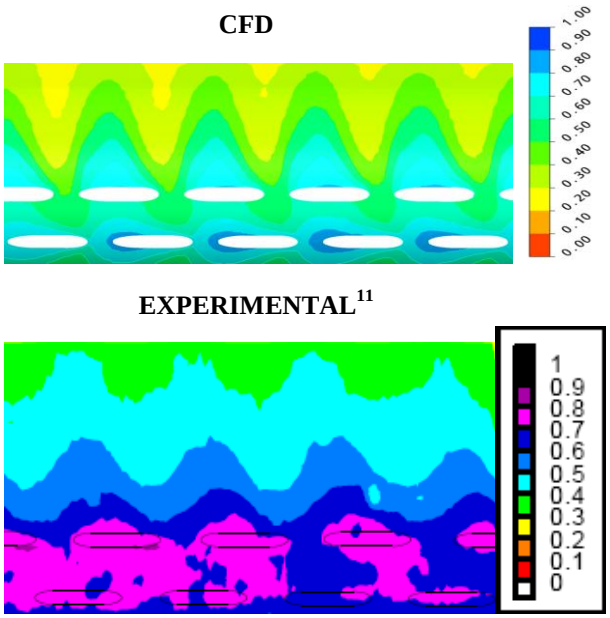

Figure 8. Overall effectiveness contours comparisons for M = 2 (M = 2.1 experimental). Experimental contours taken from [12]

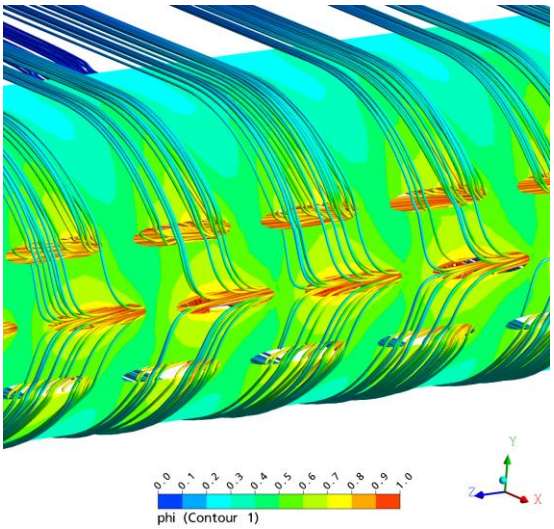

Figure 9. Overall effectiveness contours and effectiveness-colored streamlines at the leading edge for M =1

C3X Vane Model

We now turn our attention to the film cooled NASA C3X vane. Numerical solutions were obtained for both adiabatic and conjugate cases. Adiabatic conditions were prescribed on the external surface of the model and on the internal surface of the U-bend flow channel. The aft coolant flow channel and solid vane were not simulated in order to reduce the size of the computational domain. This is different from the experiments described in part I of this paper, where the test vane was constructed of polyurethane foam with a thermal conductivity k=0.048 [W/mK]. The thermal conductivity of the solid vane in the conjugate model was identical to the castable epoxy resin used in the experiments, k=1.02 [W/mK].

The behavior of the film jet as a function of the momentum ratio is depicted in Fig. 10, using contours of adiabatic effectiveness at a plane located at a film hole center. The contours suggest that there is coolant flow separation for all momentum ratios. A stronger liftoff can be observed as the momentum ratio increases. Further evidence of coolant separation can be found by inspecting the laterally averaged adiabatic effectiveness in Fig. 11. When the coolant jet separates from the wall, the laterally averaged effectiveness drops significantly immediately downstream of the hole. Experimental results start showing significant jet liftoff at I=0.75 while numerical predictions show separation at the lowest momentum ratio, I=0.34. Previous numerical investigations have shown a poor performance of RANS models in predicting the mixing of the coolant with the main stream [15,22-23]. Additionally, Kohli and Bogard [23] found significant local variations in the turbulent Prandtl number of film cooling flows when the freestream turbulence is low. One important difference between the present study and previous investigations of canonical film configurations showing poor film jet mixing in RANS models is the high curvature of the surface and corresponding large streamwise pressure gradient at the film location. Therefore, similar or more severe discrepancies in RANS predictions of adiabatic film effectiveness over a large s/d length downstream of the holes can be expected.

A similar configuration using the C3X vane but with a more complex cooling hole arrangement was by studied numerically by Laskowski et al [2]. Although numerical predictions matched the surface temperature data well, comparisons could only be made far from the hole exit where the data was available. Other differences with respect to the current setup are: two rows of suction side cooling located further downstream and fed by a plenum (the current case feeds the film from a cavity with Re=20,000) and film accumulation from showerhead film rows that were present in [2].

The numerical laterally averaged overall effectiveness comparisons against measurements are shown in Fig. 12. As for the adiabatic cases, the surface temperature increases monotonically with the momentum ratio. Since the nominal internal heat transfer rate is the same in all cases the same effectiveness trends are expected for adiabatic and conjugate cases. The agreement between CFD predictions and measurements improve with respect to the adiabatic cases due the contribution of the internal cooling and diffusion in the solid vane to the overall effectiveness.

Figure 13 depicts both numerical and experimental contours of surface effectiveness. The diffusion of heat in the matched Biot model significantly reduces the thermal gradients near the film holes. This behavior has previously been noted in a leading edge model in ref [12] and solved numerically in this paper. Both experiments and CFD show an asymmetric footprint that is attributed to the velocity of the coolant inside the forward cavity. An important difference between CFD and measurements in Fig. 13 is the distribution of the effectiveness next to the holes. While the CFD-based adiabatic effectiveness is zero between the holes, the experiments predict finite values. This is attributed to the finite conductivity of the polyurethane used in the experiments and the strong convection inside the film cooling holes.

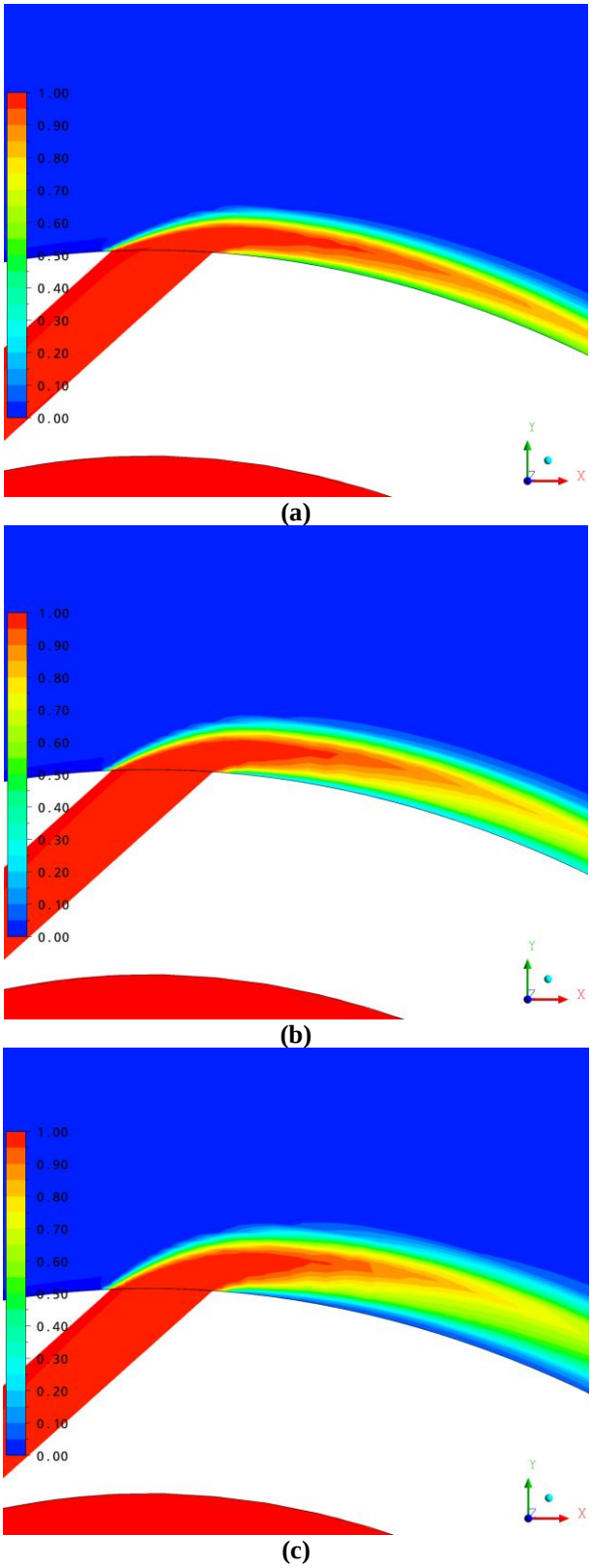

(a)

(b)

(c)

Figure 10. Adiabatic effectiveness contours at a film hole mid plane: (a) I=0.34; (b) I=0.75; (c) I=1.41

The film hole flow field depicted in Fig 14 shows a strong effect of the cavity and hole interaction. The separation bubble caused by the sharp angle formed by the hole intersection with the cavity dominates the shape of the velocity field. The flow acceleration caused by the *vena contracta* strongly affects the velocity profile at the hole breakout in the mainstream passage. The resulting locally high momentum ratio may be responsible for the coolant jet liftoff. Lin and Shih [24] consider L/D ratios smaller than 6 very likely to produce strong enough cavity-hole interactions to significantly affect the jet profile and the effectiveness of the film holes. The L/D in the present study is between 5 and 6 with an extremely sharp angle at the cavity-hole interface. It is therefore expected that small imperfections in the film hole manufacturing (i.e. non-sharp corners) can significantly change the local flow field in the hole and the distribution of the film effectiveness on the vane surface.

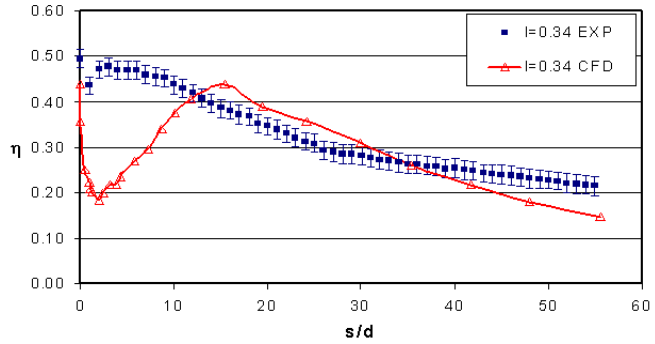

(a)

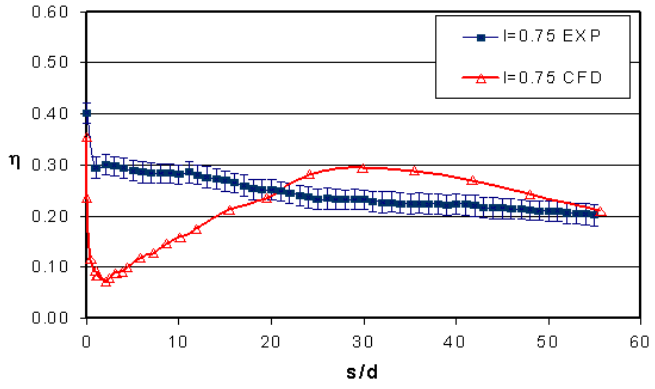

(b)

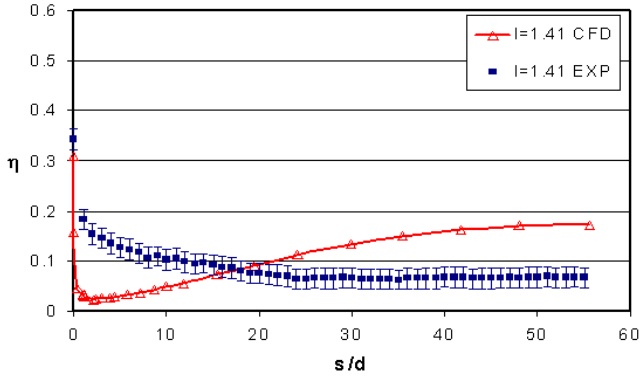

(c)

Figure 11. Laterally-averaged adiabatic effectiveness, TU=0.5%: (a) I=0.34; (b) I=0.75; (c) I=1.41

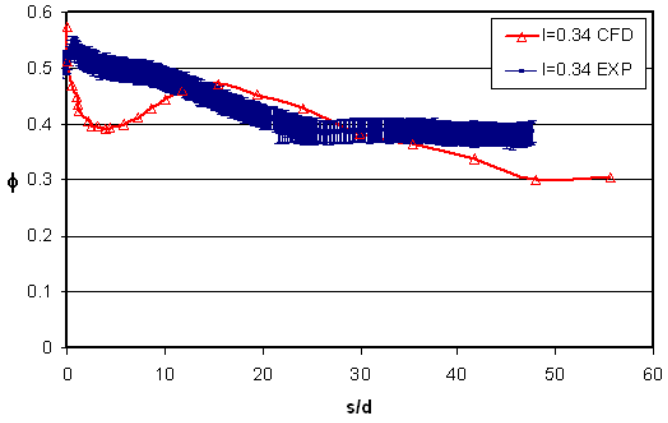

(a)

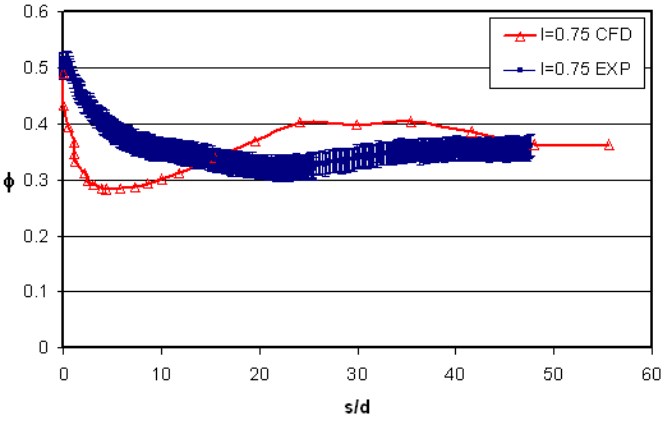

(b)

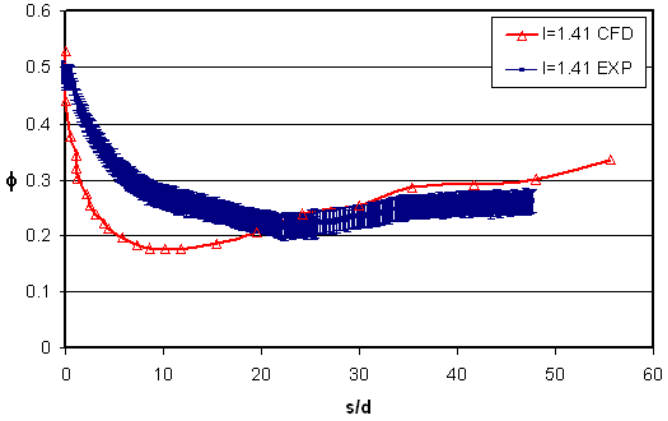

(c)

Figure 12. Laterally-averaged overall effectiveness, TU=0.5%: (a) I=0.34; (b) I=0.75; (c) I=1.41

Additional simulations using different RANS turbulence models were run using the adiabatic low momentum ratio case (I=0.34). The models used were: standard k-epsilon, Shear Stress Transport (SST) and Spalart-Allmaras (SA) one-equation model. The laterally averaged results, presented in Fig. 15, show nearly the same behavior for all models except SA. The SA effectiveness is consistently lower until S/d=35 where the curves cross. Downstream of S/d=35, the effectiveness predicted by the SA model matches the data well within the experimental uncertainty. Previous CHT studies have also similar effectiveness predictions with different RANS turbulence models [17]. Most of the limitations of RANS models in predicting film cooling have been attributed the unsteady nature of the flow, and the constant Prandtl number assumption [15,23]. Therefore, improved prediction of film cooling in realistic configurations call for more complex turbulence models that are capable of better capturing the fundamental physics of the film jet and main flow interaction.

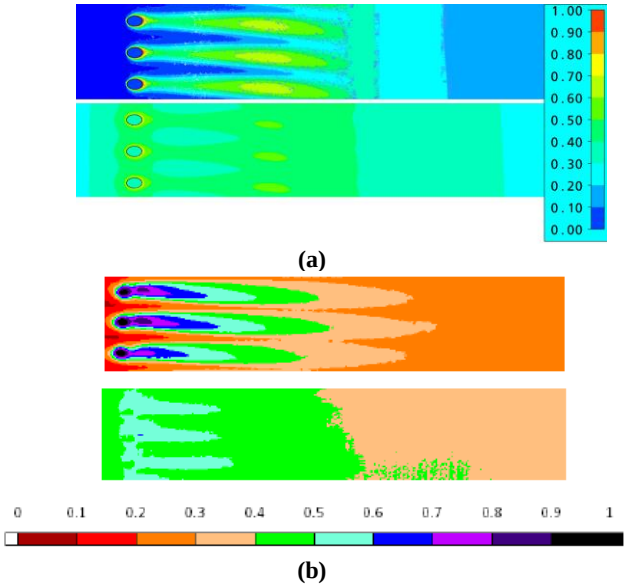

(a)

(b)

Figure 13. Effectiveness contours: (a) CFD; (b) Measurements. Top figure corresponds to adiabatic case and bottom figure corresponds to the CHT case (I=0.34). Different color maps shown in CFD results and measurements.

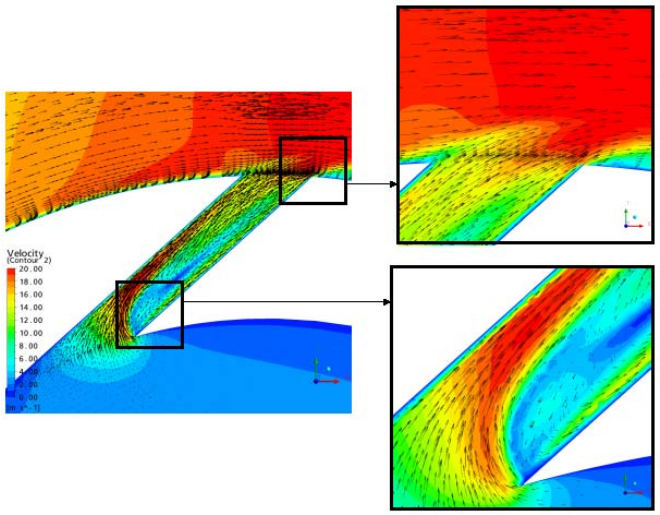

Figure 14. Film hole flow field at a XY plane across the center of the hole, I =0.34

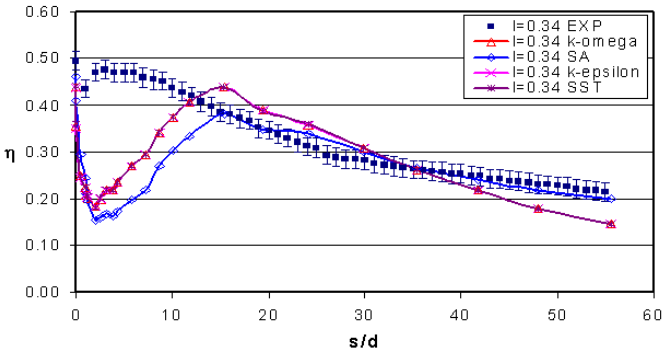

Figure 15. Effect of turbulence models on the laterally averaged adiabactic effectiveness, I=0.34

CONCLUSIONS

Coupled 3D CHT simulations were carried out for the leading edge model of Albert et al., [12] and a HPT vane with suction side film cooling. The simulations were conducted using the Wilcox k-ω turbulence model [13]. The fluid and solid domains were meshed separately. The resulting nonconforming mesh interfaces were treated with an interpolation procedure. The numerical predictions were compared against experimental data. For the leading edge model the agreement of the laterally averaged overall effectiveness with experimental data was within the experimental error downstream of the off-stagnation rows, for blowing ratios between 2 and 4. When the blowing ratio is 1, the agreement is within 22%. The numerically predicted trend of the laterally averaged effectiveness between the rows of film differs from the measured data. The experimental effectiveness remains nearly constant downstream of the stagnation row while the CFD predicts a 20% effectiveness decay. For the C3X vane with suction side film cooling, large differences (i.e. CFD underpredicts adiabatic effectiveness as much as 400% at S/d<5) between CFD and measurements were found downstream of the holes, especially when S/d<20. These differences may be attributed to RANS overprediction of coolant jet separation, isotropic turbulence and unsteady effects. Four RANS turbulence models were tested and no significant improvement was found in the prediction of the surface effectiveness near the holes. One important contribution of this article is the CHT validation effort carried out for airfoil regions with high curvature, namely the leading edge and suction side, s/d=0.21. These are commonly used film geometry that lacks open literature publications [18]. The film cooling effectiveness results in the vicinity of the film holes presented in this paper serve as a foundation for future CHT efforts.

ACKNOWLEDGEMENTS

The authors gratefully acknowledge the support of the NASA NRA program for this research and the guidance provided by the Technical Monitor Dr. J. Heidmann.

REFERENCES

[1] Bohn D.E., and Tümmers C, (2003) Numerical 3-D Conjugate Flow and Heat Transfer Investigation of a Transonic Convection Cooled Thermal Barrier Coated Cooling Fluid Mass Flow, , GT2003-38431

[2] Laskowski, G. M., Ledezma, G. A., Tolpadi, A. K., and Ostrowski, M. C. (2008) CFD Simulations and Conjugate Heat Transfer Analysis of a High Pressure Turbine Vane Utilizing different Cooling Configurations. ISROMAC12-2008-20065.

[3] Luo L., and Razinski E. H. (2007) Conjugate Heat Transfer Analysis of a Cooled turbine vane using the V2F Turbulence Model, Journal of Turbomachinery, 129:773-781.

[4] Bohn D., J. Ren and K. Kusterer, (2005) Cooling Performance of the Steam-Cooled Vane in a Steam Turbine Cascade, GT2005-68148

[5] Krüger U., Kusterer K, Lang G., Rösch H., Bohn D., and Martens E., Analysis of the Influence of Cooling Steam Conditions on the Cooling Efficiency of a Steam-Cooled Vane Using the Conjugate Calculation Technique, ASEM paper GT2001-0166

[6] Kusterer, K., Hagedorn, T., Bohn, D., Sugimoto, T., and Tanaka R., 2005, "Improvement if a Film-Cooled Blade by Application of the Conjugate calculation Technique," ASME Paper GT2005-68555.

[7] Kusterer, K., T., Bohn, D., Sugimoto, T., and Tanaka R., 2004, "Conjugate Calculations for a Film-Cooled Blade Under Different Operating Conditions," ASME Paper 2004-53719.

[8] Montomoli, F., Della Gata, S., Adami, P., and Martelli, F., 2004, "Conjugate Heat Transfer Modeling in Film Cooled Blades," ASME paper GT2004-53177.

[9] Takahashi, T., and Watanabe, K., 2005, "Conjugate Heat Transfer Analysis of a Rotor Blade with Rib-Roughened Internal Cooling Passages," ASME Paper GT2005-68227.

[10] Hylton, L D., Nirmalan, V., Sultanian, B. K., and Kaufman, R. M., (1988) The effect of leading edge and downstream film cooling on turbine vane heat transfer. NASA CR-18133.

[11] Hylton, L.D., Milhec, M.S., Turner, E.R., Nealy, D.A., and York, R.E., 1983, "Analytical and Experimental Evaluation of the Heat Transfer Distribution Over the Surface of Turbine Vanes," NASA CR 168015

[12] Albert. J. E., Bogard, and D. G., Cuhna F., 2004 "Adiabatic and overall effectiveness for a film cooled blade", ASME Paper GT2004-53998.

[13] Ansys CFX Release V11.0 (2006)

[14] Tyagi, M., and Acharya, S., (2003) Large Eddy Simulation of Film Cooling Flow from an inclined cylindrical jet, Journal of Turbomachinery, 125:734-742.

[15] Hoda, A., Acharya, S., and Tyagi, M., (2000) Predictions of a Jet-In-Crossflow with Reynolds Stress Transport Models and Large Eddy Simulations, ASME Paper GT2000-0249.

[16] Na, S., Cunha, F.J., Chyu, M.K., Shih, T.I-P., Effects of Coating Blockage and Deposit on Film Cooling Effectiveness and Surface Heat Transfer, AIAA-2006-0024.

[17] Ledezma, G.A., Laskowski, G.M., and Tolpadi, A.K., (2008) Turbulence Model Assessment for Conjugate Heat Transfer in a High Pressure Turbine Model., ASME Paper 2008-50498

[18] Bunker, R. S., (2005) A Review of Shaped Hole Turbine Film Cooling Technology, Journal of Heat Transfer, 127: 441-453.

[19] Dees, J.E., Ledezma, G.A., Bogard, D.G., Laskowski, G.M., Tolpadi, A.K., 2009, "Experimental Measurements and Computational Predictions for an Internally Cooled Simulated Turbine Vane," ASME paper IMECE2009-11622

[20] Dees, J.E., Ledezma, G.A., Bogard, D.G., Laskowski, G.M., Tolpadi, A.K., 2010, "Experimental and Computational Measurements for an Internally Cooled Simulated Gas Turbine Vane with 90 degree Rib Turbulators," ASME paper GT2010-23004.

[21] Dees, J.E., Ledezma, G.A., Bogard, D.G., Laskowski, G.M., Tolpadi, A.K., 2010, "Momentum and Thermal Boundary Layer Development on an Internally Cooled Turbine Vane," ASME paper GT2010-23008

[22] Liu, C-L, Zhu, H-R, and Bai, J-T, (2008)"Effect of turbulent Prandtl number on the computation of film-cooling effectiveness," International Journal of Heat and Mass Transfer, 51:6208-6218.

[23] Kohli, A., and Bogard, D., "Turbulent Transport in Film Cooling Flows," Journal of Heat Transfer, 127:512-520.

[24]Lin, Y-L and Shih, T.I.P., "Film Cooling of a Cylindrical Leading Edge win Injection Through Rows of Compound Angles Holes," Journal of Heat Transfer, 123:645-653

[25] Na, S., Bryden, M., and Shih, T. I-P., "CFD Analysis of Film Cooling," 44th Aerospace Sciences Meeting and Exhibit AIAA 2006-0022.

[26] Na, S., Cunha, F. J., Chyu, M. K., and Shih, T. I-P., "Effect of Coating Blockage and Deposit on Film-Cooling Effectiveness and Surface Heat Transfer, 44th Aerospace Sciences Meeting, AIAA 2006-0024.

[27] Ravelli, S., Dobrowolski, L., and Bogard, D., "Evaluating the Effects of Internal Impingement Cooling on a Film Cooled Turbine Blade Leading Edge," GT2010-23002.

[28] Dobrowolski, L., Bogard, D., Piggush, J., and Kohli, A., "Numerical Simulation of a Simulated Film Cooled Turbine Blade Leading Edge Including Conjugate Heat Transfer Effects," IMECE2009-11670.